Journal of Glaciology

Article

Cite this article: Holmes FA, van Dongen E, Kirchner N (2024). Modelled frontal ablation and velocities at Kronebreen, Svalbard, are sensitive to the choice of submarine melt rate scenario. *Journal of Glaciology* **70**, e39, 1–12. https://doi.org/10.1017/jog.2023.94

Received: 19 April 2023
Revised: 11 October 2023
Accepted: 21 October 2023

Keywords:
calving; glacier modelling; ice dynamics; ice/ocean interactions

Corresponding author:
Felicity Alice Holmes;
Email: felicity.holmes@geo.su.se

cambridge.org/jog

Modelled frontal ablation and velocities at Kronebreen, Svalbard, are sensitive to the choice of submarine melt rate scenario

Felicity Alice Holmes[1,2], Eef van Dongen[3] and Nina Kirchner[1]

[1]Department of Physical Geography, Stockholm University, Stockholm, Sweden; [2]Department of Geological Sciences, Stockholm University, Stockholm, Sweden and [3]Department of Meteorology, Stockholm University, Stockholm, Sweden

Abstract

Both submarine melt and calving are important for the overall mass balance of marine-terminating glaciers, but uncertainty is rife with regards to the magnitude of the processes. Modelling allows for these processes to be investigated without the need to visit inaccessible ice marginal zones. This study looks at the impact of different submarine melt and sea-ice back pressure scenarios on modelled calving activity and dynamics at Kronebreen, Svalbard, by running separate summer and winter simulations with various submarine melt parameterisations and sea-ice characteristics. It is found that submarine melt is an important driver of seasonal variation in modelled glacier dynamics and calving activity, with the choice of sliding law also exerting a significant influence on results.

Introduction

Despite recent progress and new insights (e.g. De Andrés and others, 2018; Ma and Bassis, 2019; Slater and Straneo, 2022), the rates of frontal ablation (the combination of calving and submarine melt) at marine-terminating glaciers are a key source of uncertainty with regards to sea-level rise projections (Moore and others, 2013). This is because in situ observations of calving and submarine melt are scarce which, in turn, hampers attempts to find good parameterisations of these processes for implementation in numerical models and leads to a situation in which there is a larger optimal range in results from simulations which include these processes. Rates of mass loss from marine-terminating glaciers have been generally increasing, with previous studies having found that ocean temperatures are, in conjunction with atmospheric temperatures, important for the frontal ablation of marine-terminating glaciers alongside the absence or presence of buttressing from sea ice or ice melange (Christoffersen and others, 2011; Luckman and others, 2015; Holmes and others, 2019; Barnett and others, 2022). An increase in frontal ablation as a result of increased oceanographic and/or atmospheric temperatures and associated failure of ice melange/sea-ice formation can have significant implications for glacier dynamics, as acceleration, thinning and retreat have been observed in response to initial perturbations (O'Leary and Christoffersen, 2013; Moyer and others, 2017; Lemos and others, 2018; Shepherd and others, 2018).

The recent Atlantification of the Arctic Ocean and the Barents Sea (Polyakov and others, 2017; Barton and others, 2018; Vihtakari and others, 2018) has led to some of Svalbard's marine-terminating glaciers becoming exposed to increasingly warmer (Atlantic) waters at their calving fronts (Vihtakari and others, 2018; Holmes and others, 2019), making them interesting sites for investigating the impacts of warm water intrusion on glacier dynamics. Svalbard is also impacted by increasing atmospheric temperatures, with these increases predicted to play a role in a doubling of mass loss by 2100 (Geyman and others, 2022). Calving has been estimated to be responsible for 17–25% of mass loss on Svalbard (Błaszczyk and others, 2009), although more up-to-date studies are needed to better constrain these numbers (Schuler and others, 2020). Many disparate processes are related to the ice–ocean boundary, for example increased air temperatures will cause more glacial run-off of which parts will end up at the glacier base and contribute to subglacial discharge. This, in turn, may feed meltwater plumes at calving fronts which can turbulently entrain glacier proximal warm Atlantic waters and bring them into contact with the ice front to cause elevated levels of frontal melt (Motyka and others, 2003) which can cause undercutting and promote calving at the glacier terminus (How and others, 2019). Bathymetry is also influential in determining the retreat of any given glacier (e.g. through the existence of pinning points), and can be instrumental with regards to whether warm waters are able to reach the glacier fronts (Weertman, 1974; Carr and others, 2015; Jakobsson and others, 2020). Even if it can be determined whether or not warm waters are reaching the calving fronts of glaciers, it is not an easy task to measure the magnitude of frontal melt or how this may in turn affect calving. This is where modelling studies can be instrumental in allowing the processes at the ice–ocean boundary to be thoroughly investigated. Kronebreen, which is the focus of this paper, is not subjected to large amounts of ice melange back pressure, but can be impacted by the presence of fast sea ice during winter with potential implications for frontal ablation (Pavlova and others, 2019).

Specifically, the average maximum thickness of fast ice in Kongsfjorden was found to be ~0.6 m pre-2006, after which it has declined to ~0.2 m (Pavlova and others, 2019). Previous modelling work has shown that increased levels of submarine melt and undercutting are often accompanied by elevated calving fluxes and are important for reconstructing observed behaviour (Todd and others, 2018; Vallot and others, 2018; Ma and Bassis, 2019), but that back stress from ice melange can play an important role in reducing calving fluxes (Krug and others, 2015; Barnett and others, 2022). This study simulates Kronebreen during both summer 2016 and winter 2016–17 using a three-dimensional (3-D) model in order to quantify the impact of different submarine melt rate parameterisations on calving activity, frontal ablation and glacier dynamics. In addition, winter simulations are set-up to isolate the impacts of sea-ice back pressure on Kronebreen's behaviour. As such, the aim of the paper is to gain insights into the processes impacting modelled calving dynamics over seasonal timescales, rather than to create an accurate analogue of Kronebreen.

Study area

This study focuses on Kronebreen, which is a fast-flowing glacier situated on Svalbard's west coast at 78.8N (see Fig. 1). The glacier is polythermal and of surge type, although it is currently in a quiescent phase (Błaszczyk and others, 2009). The calving front of Kronebreen is ~3.6 km wide, and terminates in Kongsfjorden. The height of the grounded terminus is most often between 100 and 150 m, with ~50–60 m of the calving front being above the waterline. There is no pronounced sill in Kongsfjorden (Promińska and others, 2017), and Atlantic water has been observed near Kronebreen's calving front in 2014 and 2016 (Promińska and others, 2017; Holmes and others, 2019). However, the physical environment of Kongsfjorden varies both seasonally and inter-annually with cold Arctic waters and glacial melt also being present (Svendsen and others, 2002; Cottier and others, 2005). Various estimates for frontal melt rates at Kronebreen have been suggested over recent years, with winter lows ranging from ~30 to ~400 m a^{-1} and summer highs ranging from ~300 to ~2300 m a^{-1} between studies (Holmes and others, 2019; Köhler and others, 2019). A recent estimate found that frontal ablation accounted for ~84% of total mass loss at Kronebreen for the period 2009–14 (Deschamps-Berger and others, 2019). Kronebreen has additionally been subject to an increasingly negative surface mass balance (SMB) in recent decades, with supra-glacial melt being 21% higher between 2000 and 2012 than between 1961 and 1999 (Van Pelt and others, 2012). Previous modelling work at Kronebreen has indicated that undercutting is of great importance for calving, with modelled retreat only matching observed retreat when undercutting is included (Vallot and others, 2018).

Methods

Model set-up

For the simulations presented in this paper, Elmer/Ice version 9.0 was used. This is an open source finite-element, full-Stokes, ice-sheet model (Gagliardini and others, 2013) (github.com/ElmerCSC/elmerfem).

The mesh outline, as well as the inversions, spin-up and relaxation simulations, are the same as described by Holmes and others (2023). Following this, the main suite of simulations were run at a time step of 0.25 d and each simulation was run for 3 months. This corresponds to the period July 2016 until the end of September 2016 for the summer simulations and the period December 2016 until the end of February 2017 for the winter simulations. Separate summer and winter simulations were run as the drivers of calving vary with season as a result of changes in both submarine melt and the presence of sea-ice back pressure. These periods were chosen as they both correspond to time periods for which data relating to both external meteorological parameters and glacier dynamics are available (see Holmes and others, 2019). The Calving3D solver, developed and presented by Todd and others (2018), was used for all the experiments. Here, calving occurs when either surface crevasses propagate down to sea level or when surface and basal crevasses join up. These criteria are based on the calving depth criterion as described by Benn and others (2007). After a calving event occurs, the model domain is remeshed to reflect the change in geometry (Todd and others, 2018).

Model forcings and inputs

There are five different types of boundary in the model (bedrock boundary, ice–atmosphere boundary, ice–ice boundary, ice–rock boundary and the calving front – see Fig. 2).

At the ice–atmosphere boundary, which was allowed to evolve with time, SMB is applied as a forcing. Here, daily values corresponding to the 2016/17 study periods are used (Noël and others, 2020).

At the bedrock boundary, most of the simulations employed a Weertman (1974) type sliding law with basal friction prescribed as a temporally constant but spatially variable value, corresponding to the separate summer 2016 and winter 2016–17 inversions performed and described by Holmes and others (2023). This approach has been used widely for simulations of calving in Elmer/ice (Todd and others, 2018, 2019; Cook and others, 2020), and the importance of having basal friction fields from the correct season and year was highlighted by Vallot and others (2017). As a Weertman sliding law was reported to be potentially problematic during summertime (Vallot and others, 2017), all the summer simulations were also run with a Coulomb type sliding law – although it must be noted that there are uncertainties with this, too, as basal water pressures are not well constrained (Vallot and others, 2017). A no-penetration condition was also set for this boundary.

At the ice–ice boundaries, velocities were set to equal satellite-derived surface velocity observations. In contrast, velocities were set to zero at the ice–rock boundaries and a no-penetration condition was enforced.

At the calving front, frontal melt was applied to the submarine parts of the terminus, with the magnitude of this melt being spatially heterogeneous in some simulations in order to emulate plumes. Plume locations were based upon where plumes could be observed on optical satellite images, and are only present in certain summer simulations (see Fig. 1). The submarine melt rate is variable with time during the simulations, with this variation based upon a time series of water temperatures at a depth of 67 m collected ~1 km from the calving period of Kronebreen during August 2016–September 2017. This dataset is presented in more detail by Holmes and others (2019). For use in the model, the time series was normalised between 0 and 1 and written to a netCDF file. From here, the data could be read into Elmer/Ice and used as a basis to create a number of different frontal melt scenarios, by multiplying the normalised value by a seasonal factor which determined the maximum melt rate, in a similar way to how glacial index scaling has been used to force other models (e.g. Clason and others 2014). The summer simulations used water temperature variation data from summer 2016, and the winter simulations used water temperature variation data from winter 2016–17.

https://doi.org/10.1017/jog.2023.94 Published online by Cambridge University Press

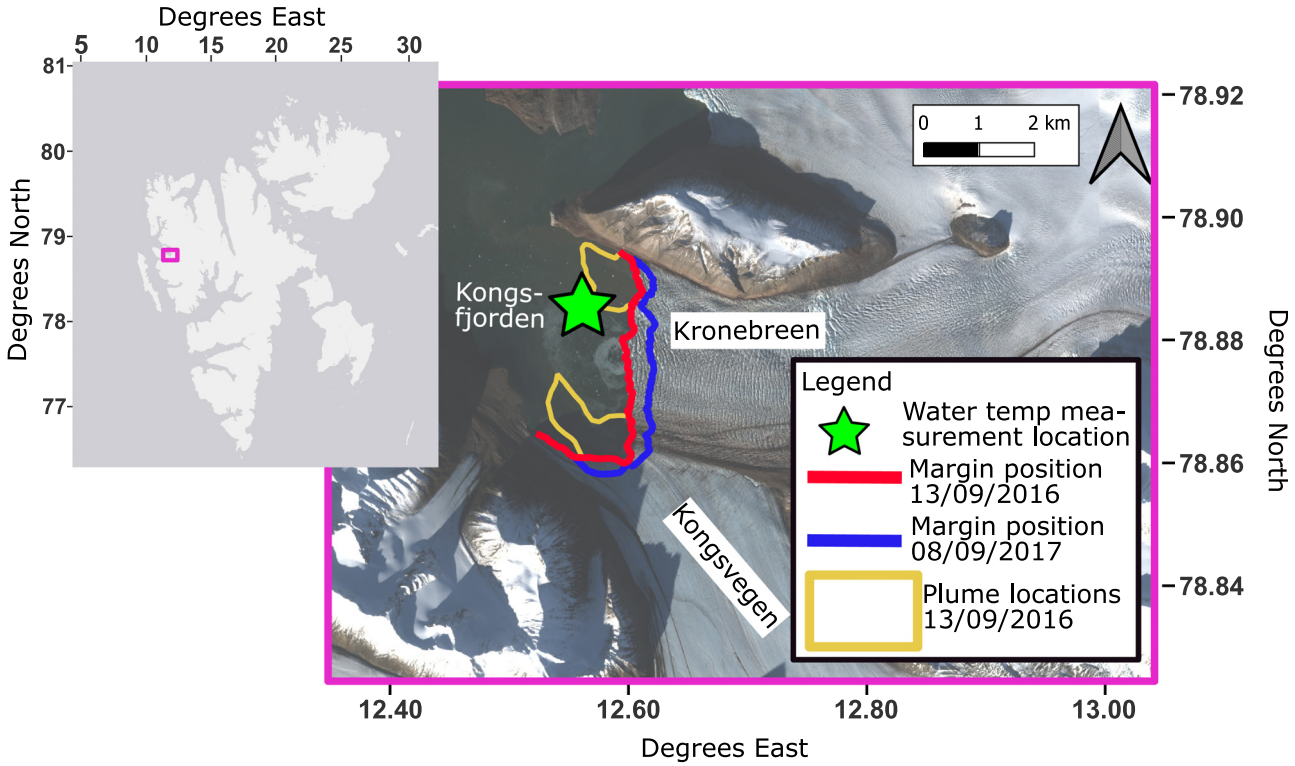

Figure 1. Inset: Map of Svalbard showing location of Kronebreen (pink box). Main image: Map of Kronebreen showing margin positions in September 2016 (red) and September 2017 (blue), as well as the location of plumes at the calving front (yellow). The neighbouring glacier Kongsvegen and the fjord Kongsfjorden are also shown. The distance between the 2016 and 2017 margins is, on average, 400 m. Background for the main image is Copernicus Sentinel data (2016), retrieved from Copernicus Open Access Hub 02/08/2022 and processed by ESA. Background for inset image from source: Esri, DeLorme, HERE, MapmyIndia.

Back pressure from sea ice was also prescribed at the calving front in some simulations. The timing of this buttressing force was based upon daily records of sea-ice fraction in Kongsfjorden from the Norwegian Ice Service. The buttressing force on Kronebreen has not been quantified previously and a number of different possible scenarios were investigated here (see Section 'Experimental design'). The buttressing force presented for each scenario in Table 1 is the back stress per metre of sea ice (σ_M, kPa), which is related to the overall buttressing force (σ_{fb}, kPa) by the following equation (as used by e.g. Todd and Christoffersen, 2014; Barnett and others, 2022):

$$\sigma_M = \sigma_{fb} \frac{H_{T.Avg}}{H_M}. \quad (1)$$

Here, the mean terminus height is denoted by H_T.Avg (~125 m for Kronebreen) and the mean sea-ice thickness by H_M.

Experimental design

The simulations were designed in order to investigate the sensitivity of modelled calving activity and glacier dynamics to different submarine melt and sea-ice back pressure scenarios. Specifically, submarine melt was varied during the different summer simulations and sea-ice back pressure, which is not present during summer, was varied during the different winter simulations. All the simulations are summarised in Table 1.

In all the summer simulations, basal friction was either set equal to the results of a summer inversion (Holmes and others, 2023) or a Coulomb type sliding law was used with the friction coefficient scaled to match observed velocities at Kronebreen (e.g. as done by Joughin and others 2019). In addition, the top free surface of the glacier was forced with daily SMB values from July to September 2016 (Noël and others, 2019). The different summer simulations were, however, forced with different submarine melt rates (see Fig. 3). The scenarios chosen are within the range of previously published estimates of melt rates from the area, with summer highs of up to 1500 m a^{-1} (e.g. Holmes and

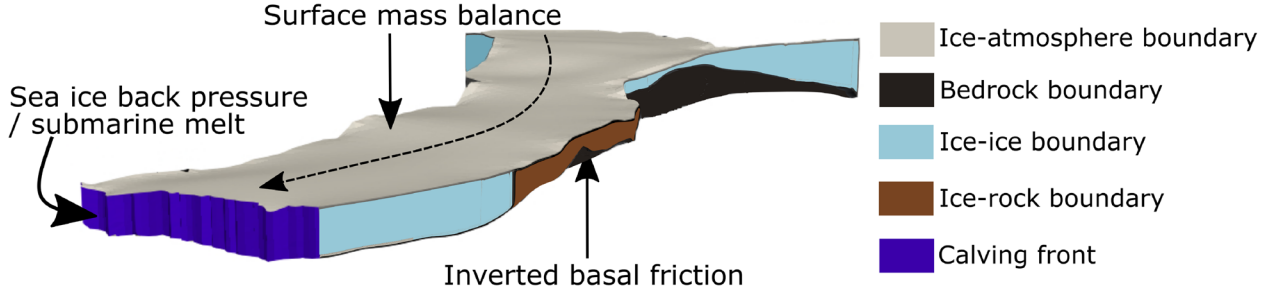

Figure 2. Geometry of Kronebreen used for the simulations, with the dashed line indicating the direction of flow. The different boundary types are denoted by the different colours. The forcings applied to the model are also present, with arrows showing which surfaces/boundaries they are applied to.

https://doi.org/10.1017/jog.2023.94 Published online by Cambridge University Press

Table 1. Summary of forcings applied in each of the main suite of simulations

Sim name	Max melt rate m a^{-1}	Melt variation	SI back pressure kPa	SI thickness m
$Summer_1$	1500	C	–	–
$Summer_2$	1500	H	–	–
$Summer_3$	1500	H and V	–	–
$Summer_4$	1500	V	–	–
$Summer_{control}$	–	–	–	–
$Summer_{coulomb1}$	1500	C	–	–
$Summer_{coulomb2}$	1500	H	–	–
$Summer_{coulomb3}$	1500	H and V	–	–
$Summer_{coulomb4}$	1500	V	–	–
$Summer_{coulombControl}$	–	–	–	–
$Winter_1$	500	C	100	0.6
$Winter_2$	500	C	100	5
$Winter_3$	500	C	50	0.6
$Winter_4$	500	C	50	5
$Winter_{control}$	500	C	–	–

Melt rate style across the entire submerged calving front is denoted by 'C' (constant), 'H' (horizontal variation) and 'V' (vertical variation). See Figure 3 for graphical representations. Sea ice is abbreviated to 'SI' in the table headers.

others, 2019; Köhler and others, 2019). One simulation, $Summer_1$ has a maximum melt rate of 1500 m a^{-1} with the same melt rate exerted across the entire submarine ice cliff – a constant melt rate (Fig. 3a). The observation of plumes from optical satellite imagery suggests that there is some horizontal variation in submarine melt rates. As such, the $Summer_2$ has the same maximum melt rate of 1500 m a^{-1}, and with half of this value (750 m a^{-1}) applied at no-plume areas (Fig. 3b). Additional data from sound velocity profiles near Kronebreen and multibeam/LiDAR derived profiles of Kronebreen's frontal geometry indicate that melt rates are variable with depth (Holmes and others, 2019, 2023). Specifically, higher melt rates may be found at the base of the calving front at ~50–60 m depth (likely due to subglacial discharge), and at ~20 m depth (likely due to high water temperatures here, as identified from the sound velocity profiles). Therefore, the $Summer_3$ simulation includes both horizontal variations in melt (plumes) and vertical variations in melt (Fig. 3c). These vertical variations in melt occur in both plume and non-plume locations. Once again, the maximum melt rate is still 1500 m a^{-1} which occurs in plume locations near the base of the glacier and at depths of 20–25 m. A melt rate of 750 m a^{-1} occurs at all other depths in plume locations, and at non-plume locations near the base of the glacier as well as between 20 and 25 m depth. At all other non-plume locations, the melt rate is 375 m a^{-1}. All the above parameterisations lead to an angular modelled undercut around the waterline and so, in order to assess the behaviour of the model in the presence of a more gradual undercut geometry, the $Summer_4$ simulation has a melt rate that gradually increased from 0 m a^{-1} at the waterline up to 1500 m a^{-1} at a depth of 50 m (Fig. 3d). Finally, the $Summer_{control}$ simulation does not include any submarine melting and serves as a control from which to assess the impact of the different melt scenarios. As the maximum melt rate was the same for all summer melt rate scenarios, the less complex scenarios such as $Summer_1$ had a greater area over which the highest melt rates could occur and thus had a greater mean submarine melt rate than the more complex scenarios such as $Summer_3$.

In all the winter simulations, basal friction was set equal to the results of the winter basal inversion from Holmes and others (2023), and the top free surface of the glacier was forced with daily SMB data from December 2016 to February 2017 (Noël and others, 2019). In addition, all winter simulations were forced by a simple frontal melt parameterisation where the magnitude of submarine melt was the same across the entire submarine ice cliff with a maximum melt rate of 500 m a^{-1}. The difference between the winter simulations was the sea-ice back pressure scenario, with both the thickness of the sea ice and the pressure exerted by the sea ice being varied (see Eqn (1)). For the depth over which pressure is exerted, the minimum value of 0–0.6 m was chosen to correspond with that published by Pavlova and others (2019). A greater depth range of 0–5 m was chosen for the 'thick' sea-ice scenario, in order to investigate the sensitivity of Kronebreen's dynamics to changes in sea ice. The buttressing force is less well constrained and values of 50 and 100 kPa were chosen for this study, with the aim that the results can be used to provide an indication of how important sea-ice back pressure is for Kronebreen. All combinations of sea-ice thickness and back pressure are simulated, and these are summarised in

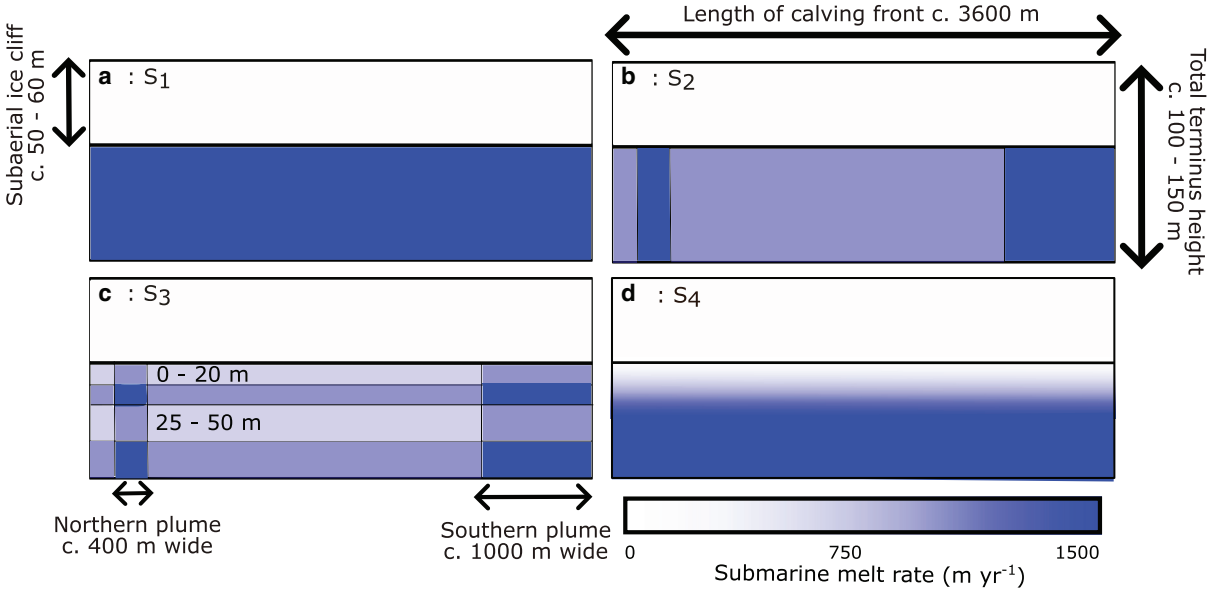

Figure 3. Different melt scenarios prescribed for the summer simulations. Panel a shows $Summer_1$, where submarine melt rates are constant across the glacier. Panel b shows $Summer_2$, where some horizontal variation in submarine melt rate is prescribed. Panel c shows $Summer_3$, where both vertical and horizontal variations in melt rate are prescribed. Panel d shows $Summer_4$, where gradual vertical melt rate variations are included to create a gradual undercut.

https://doi.org/10.1017/jog.2023.94 Published online by Cambridge University Press

Table 1. A control simulation, $Winter_{control}$, was additionally run, with no sea-ice back pressure exerted on the glacier terminus.

Model output

Several different outputs are generated by the model, and these are described in more detail below.

The position of the margin is extracted from the model at the beginning and the end of each simulation. This allows for the total margin change during the course of each model run to be compared. The starting margin position is the same for all simulations and, as a result of calving and frontal melt in the relaxation simulation, is similar to the observed September 2016 position.

A velocity field for the entire glacier (e.g. at all depths) is produced for every modelled time step. For data analysis, these data are processed to produce a time series of the mean frontal velocity for each simulation. The frontal region is defined as all nodes within 1 km of the calving front. In addition, the maximum frontal velocity for each simulation is calculated in order to provide information on any localised speed-ups.

The volume of each modelled iceberg calved from Kronebreen during a simulation is calculated by the Elmer/Ice Calving3D solver and can be written to a results file. In addition, the volume loss from submarine melt can be calculated by multiplying the submarine melt rate (in $m\,a^{-1}$) at each element by the time step size, and then by the area of the ocean-facing side of the gridcell. After the results for each element are summed, the total submarine melt volume loss from each time step is known and a time series can be created. Both the calving loss and submarine melt loss time series can be summed to give an overall figure for the volume loss.

Finally, the 3-D post-calving mesh for each time step is produced as an output, allowing for the changes in frontal morphology with time to be visualised by plotting profiles from these meshes.

Results

The results from all the summer and winter simulations can be compared to each other to provide information on model behaviour and sensitivity. In addition, comparison of model output and observational data can provide insights into the fidelity of the model set-up.

The results are presented beginning with large-scale trends (margin change and glacier dynamics), before focusing on the relative contribution of calving and submarine melt to frontal ablation, the differences in frontal morphology between the summer simulations, the impact of sea-ice back pressure on glacier behaviour and the impact of the choice of sliding law.

Margin change

The margin positions at the beginning and end of all simulations are shown in Figure 4, with changes in the modelled position of the terminus being owed to both submarine melt and calving activity. During the Weertman summer simulations, a retreat of ~500 m was seen in all simulations except for the $Summer_{control}$ simulation, where little margin change was modelled. For the simulations which showed significant retreat, an average retreat rate of ~5.5 $m\,d^{-1}$ was obtained. However, the central parts of the glacier retreated more than this and retreat rates of up to ~9 $m\,d^{-1}$ were simulated in these locations. The difference in margin change between the different summer simulations is small, with all the final configurations being similar. In the Coulomb summer simulations, the control simulation showed significantly more retreat than in the Weertman control simulation, with an average retreat rate of ~4 $m\,d^{-1}$. All the other simulations showed a very similar overall retreat to the Weertman simulations.

During the winter simulations, a general trend of retreat at the northern section of the glacier front was seen, along with advance at the southern end of the glacier front where there is a confluence of the glacier with Kongsvegen. The greatest levels of advance were seen in the $Winter_1$ simulation, where parts of the glacier had advanced by ~340 m (~3.7 $m\,d^{-1}$) by the end of the 3 month period. The greatest levels of retreat were seen in the $Winter_2$ and $Winter_{control}$ simulations, with a retreat of nearly 100 m total across parts of the northern section of the glacier front.

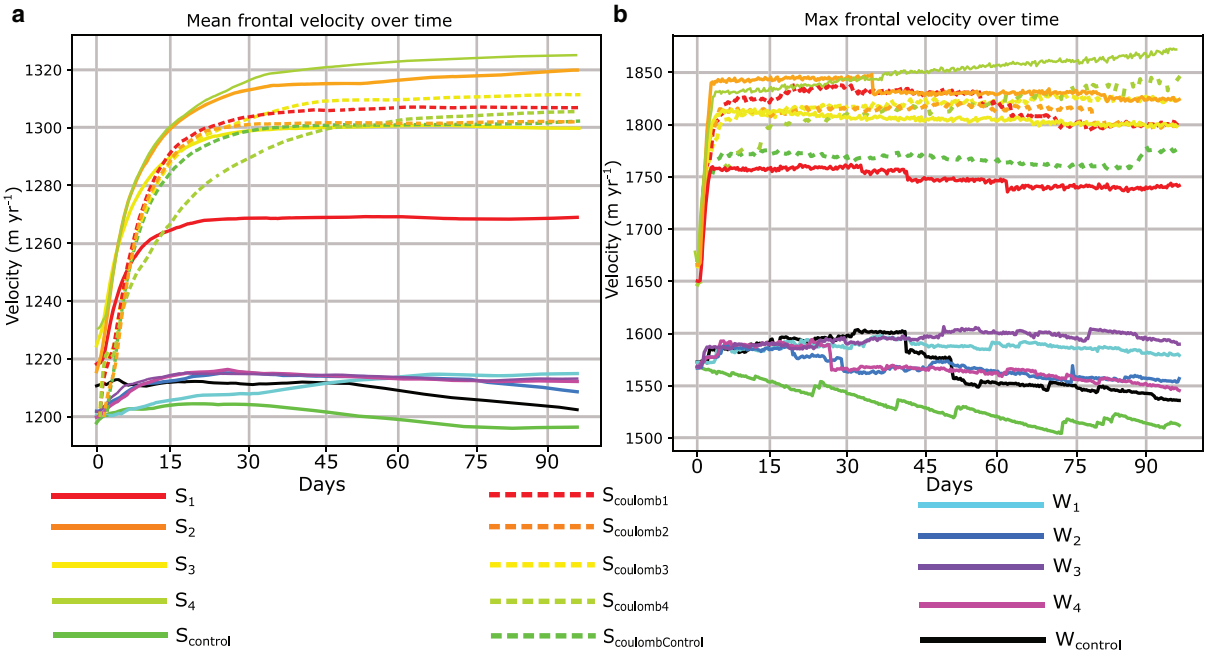

Figure 4. Margin change in the summer Weertman simulations (panel a), summer Coulomb simulations (panel b) and winter simulations (panel c), overlain on a satellite image of Kronebreen from September 2016. The black line in all panels represents the starting margin position in all simulations. The other lines represent the final margin positions after all the 3 month simulations. Background image is from source: Copernicus Sentinel data 2016. Retrieved from Copernicus Open Access Hub 02/08/2022, processed by ESA.

https://doi.org/10.1017/jog.2023.94 Published online by Cambridge University Press

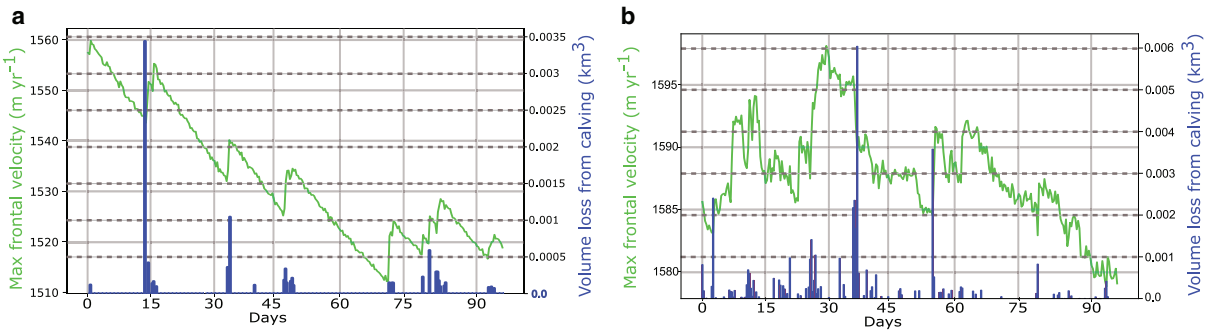

Figure 5. Frontal velocities during the course of all 3 month simulations. Panel a shows the mean frontal velocity in each simulation. Panel b shows the maximum frontal velocity in each simulation.

Glacier dynamics

Modelled mean frontal velocities (Fig. 5a) in the majority of the Weertman summer simulations accelerated at the beginning of the simulation, before becoming reasonably stable between 1260 and 1340 m a^{-1} (3.4 and 3.7 m d^{-1}). The exception to this was the Summer$_{control}$ simulation, where mean velocities remained lower at ~1200 m a^{-1} (3.3 m d^{-1}). This is similar to the winter simulations, where all the mean velocities remained ~1210 m a^{-1} (3.3 m d^{-1}).

The maximum frontal velocities (Fig. 5b) show a similar pattern to the mean velocities; all Weertman summer simulations except for Summer$_{control}$ show higher velocities than the winter simulations. However, in contrast to the other simulations where maximum velocities stabilise, the Summer$_4$ simulation shows increasing maximum velocities during the entire simulation. Here, the Summer$_{control}$ simulation clearly has the lowest maximum velocities, even when compared to the winter simulations. In most simulations, the time series of maximum velocities show clear step changes. These step changes can correspond to step increases in velocity overlain on an otherwise general trend of deceleration, as is seen most clearly in the Summer$_{control}$ simulation. Other simulations instead show step decreases in maximum velocity.

The trend of deceleration alongside sudden and short-lived velocity increases most clearly exemplified by the Summer$_{control}$ simulation is shown in more detail in Figure 6. Here, the calving losses at each time step can also be seen and it is apparent that the sudden and short-lived increases in velocity correspond with the occurrence of calving events. This pattern of small step changes is not seen in the time series of mean velocities.

Comparisons between the Weertman summer simulations and the Coulomb summer simulations show that velocities were similar regardless of sliding law. However, the Summer$_{Coulomb1}$ simulation had noticeably higher mean and maximum velocities than the Summer$_1$ simulation, and the Summer$_{CoulombControl}$ simulation was, in contrast to the Summer$_{control}$ simulation, dynamically much more similar to the simulations which included submarine melt.

Relative contribution of calving and submarine melt to frontal ablation

The relative contribution of submarine melt and calving can be compared for each simulation, as is shown in Figure 7. These data additionally give an insight into how different melt rate parameterisations impact modelled calving activity.

Most of the summer simulations showed a significantly higher mass loss from calving compared to submarine melt – with Summer$_{control}$ being the only exception. The total mass loss from the Weertman Summer$_{1, 2, 3 and 4}$ simulations was much higher than for the winter simulations, with most of the additional mass loss being due to much higher calving losses. The highest calving losses are seen in the Summer$_4$ simulation, where only vertical differentiation in melt rates was included. The lowest calving losses in the non-control simulations are seen in the Summer$_1$ simulation, where submarine melt rates were constant across the entire glacier front. The only summer simulation that did not show high calving mass losses was Summer$_{control}$ simulation, where no submarine melt was prescribed and overall mass loss was low.

The Coulomb summer simulations had slightly higher overall mass losses than the Weertman simulations, but also exhibited the pattern of very high calving losses. However, calving losses were also high in the Summer$_{CoulombControl}$ simulation, unlike the very low calving losses seen in the Summer$_{control}$ simulation.

In contrast, the relative contributions of calving and submarine melt to ice loss in the winter simulations are of the same magnitude. The mass loss is slightly higher in the Winter$_{control}$ simulation than the other simulations, with this being the simulation where no sea-ice buttressing is included in the model. The overall ice loss was similar for all winter simulations at ~0.12 km^3. The overall mass loss from the Winter$_{control}$ simulation is higher than from the Summer$_{control}$ simulation as frontal melt is still applied during the winter control simulation whereas no frontal melt is applied in the Summer$_{control}$ simulation. This is a consequence of sea-ice back pressure being the independent variable in the winter simulations as opposed to the summer simulations, where frontal melt is instead the independent variable.

Variations in frontal morphology

The frontal morphology of Kronebreen at the end of the summer simulations varied depending on the melt parameterisation used, with example profiles shown in Figure 8. In all the non-control simulations except for Summer$_3$, a single undercut is seen, with the sub-aerial section of the ice cliff projecting out over the submarine section. For the Summer$_1$ simulation, the magnitude of the undercut was ~45 m across the whole glacier front by the end of the 3 month simulation. In the Summer$_2$ simulation, the mean magnitude of the undercut was 25 m – but this was higher in plume areas. The mean undercut size was similar to this in the Summer$_4$ simulation, but here the geometry is less angular.

The frontal morphology was more nuanced in the Summer$_3$ simulation. Here, an undercut is seen at the waterline, followed by a further undercut at the base of the ice cliff. Overall, a total undercut of ~20 m is seen. At plume locations, the size of this undercut was instead ~40 m.

Undercuts also developed in the winter simulations but, as submarine melt was constant across the entire submerged calving

https://doi.org/10.1017/jog.2023.94 Published online by Cambridge University Press

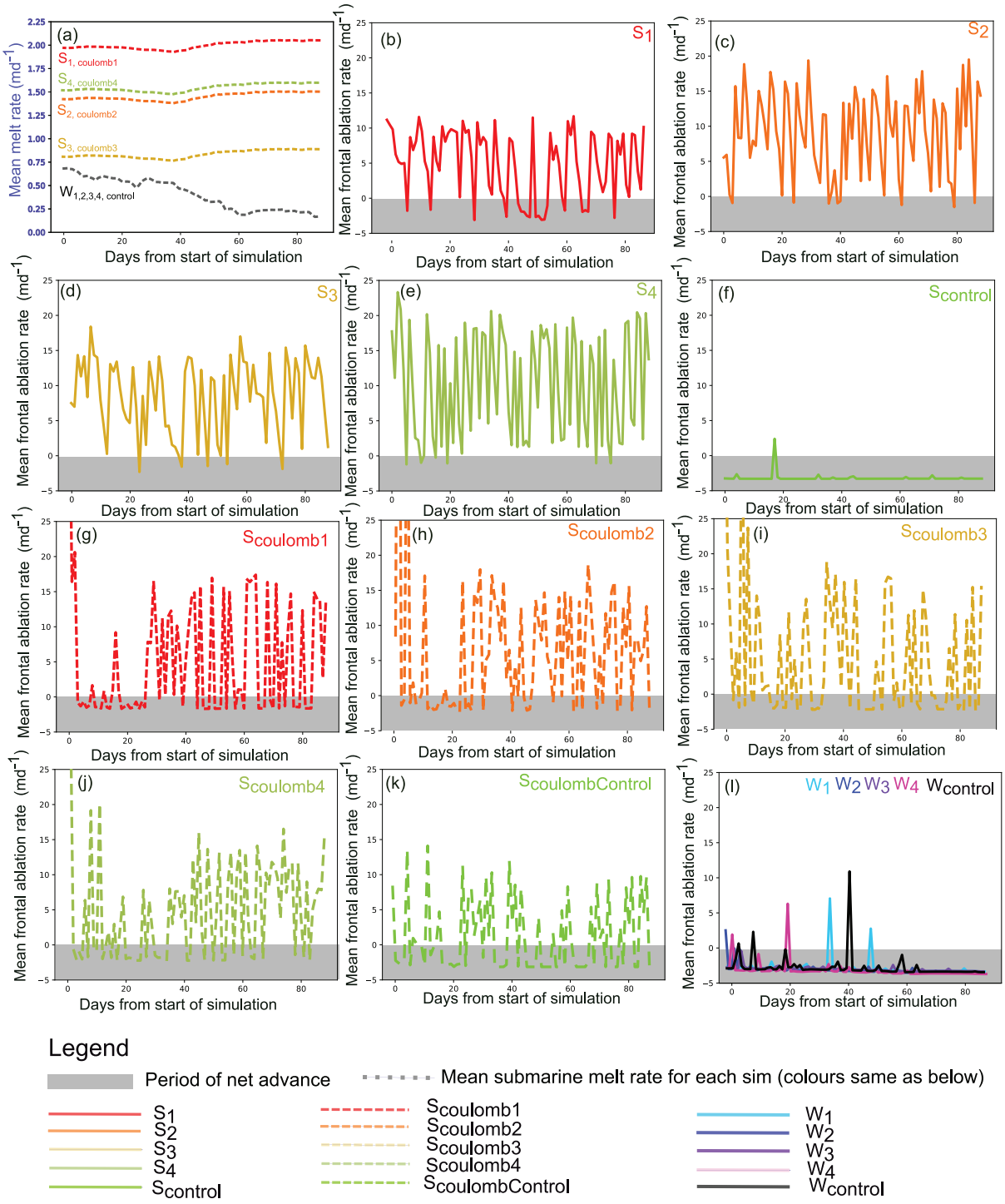

Figure 6. Maximum frontal velocities (green) and volume mass loss from calving (blue) during the $Summer_{control}$ simulation. Upticks in maximum velocity can be seen to coincide with time steps where there are modelled calving events.

front and did not vary between simulations, the undercut size was less than 10 m in all locations and is not shown.

Discussion

The impact of high submarine melt rates during summer

The fact that total mass loss and margin change is much greater during the non-control Weertman summer simulations than the Weertman control simulation suggests that melting of the calving front below the waterline is instrumental in causing high levels of frontal ablation during summer (see Figs 4, 7). The relative contribution of submarine melt and calving to total mass loss in the summer simulations shows that calving losses are much higher than submarine melt, accounting for up to 98% of frontal ablation in the model. This is a contrast to previous research which highlights the dominant role of submarine melt over calving (e.g. Bartholomaus and others, 2013). However, as the modelled calving only occurs in the presence of high levels of submarine melt, it can be seen as evidence of high levels of melt-driven mass loss – even if the extend of this undercut-driven calving is likely exaggerated by the model. This suggests that undercut-driven calving is particularly important at Kronebreen; a similar finding to that of An and others (2021), who studied Zachariae Isstrøm and found that undercutting of grounded ice in numerical models

https://doi.org/10.1017/jog.2023.94 Published online by Cambridge University Press

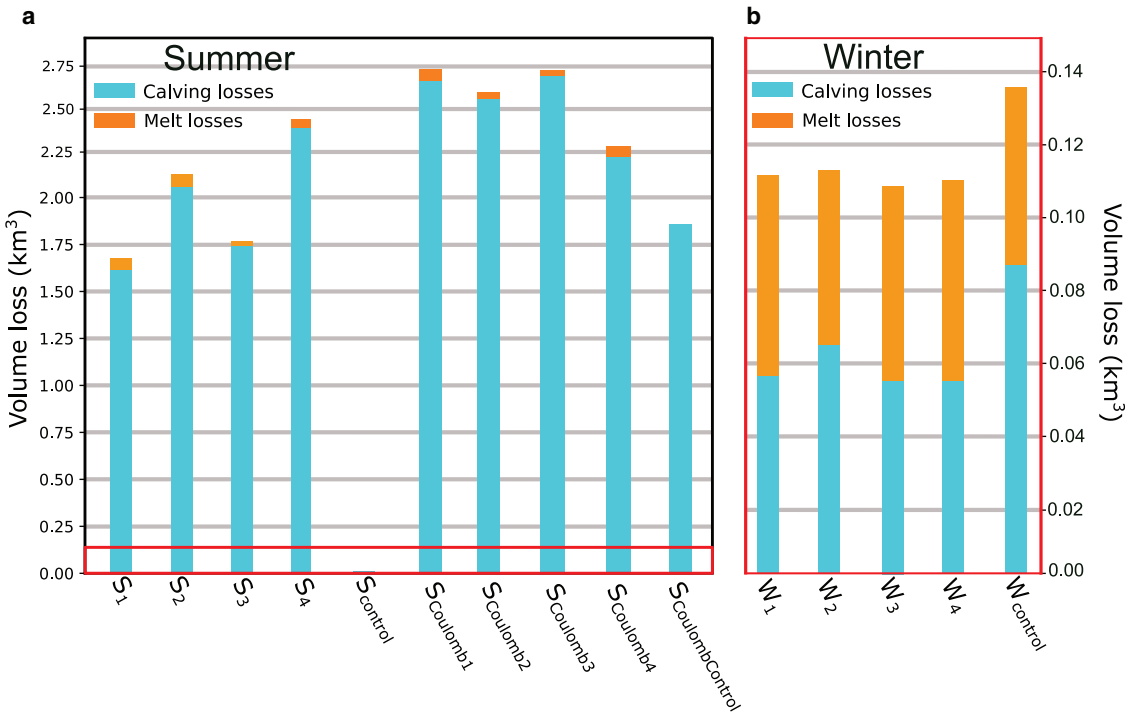

Figure 7. Total volume loss during the entirety of each simulation, broken down into loss from calving events (blue) and loss from submarine melt (orange).

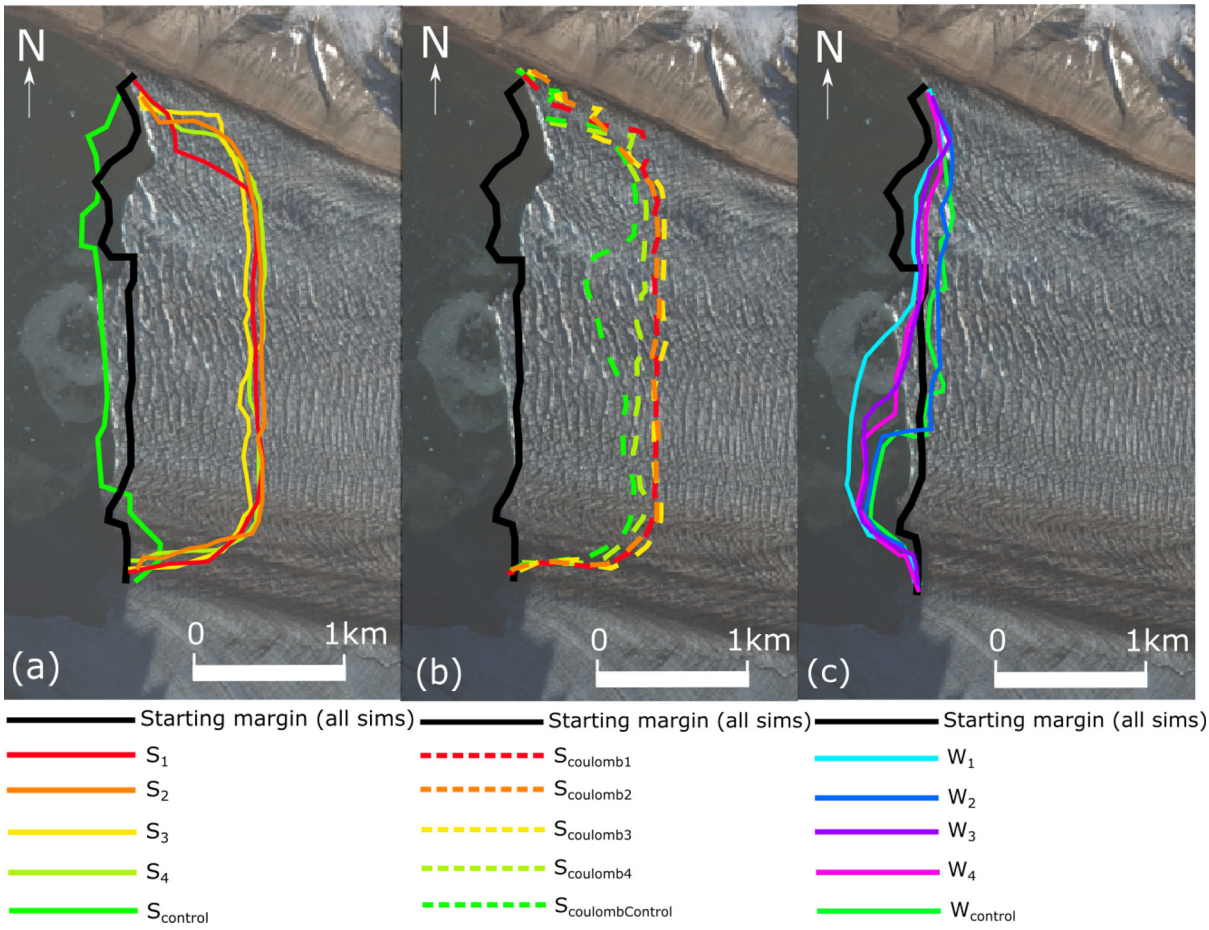

Figure 8. Modelled undercuts at the end of the 3 month summer simulations. The horizontal dashed line denotes the water level and the vertical dashed line denotes the glacier front. Results are shown from non-plume locations in all simulations. The largest undercut is seen in $Summer_1$, where the maximum melt rate was prescribed over the entire submerged calving front. $Summer_2$ shows a similar shape to $Summer_1$, but with a smaller undercut magnitude. A complex geometry with two distinct undercuts is seen in $Summer_3$, and a less angular undercut can be seen in $Summer_4$.

https://doi.org/10.1017/jog.2023.94 Published online by Cambridge University Press

was a necessary condition in order for observed high retreat rates to be reproduced. This linkage between submarine melt and calving has been additionally identified in observations, with summer calving at Yahtsee Glacier, Alaska, being a direct response to submarine melt-driven undercutting (Bartholomaus and others, 2013).

Out of the Weertman simulations, mass loss was highest for the $Summer_4$ simulation, where only vertical variation in submarine melt was included (Fig. 7). This may suggest that the vertical differentiation in melt promoted calving, but may also be related to the fact that a larger proportion of the calving front was subject to the maximum melt rates than in the $Summer_2$ and $Summer_3$ simulations. However, mass losses in $Summer_4$ were still higher than mass losses in $Summer_1$, where the maximum melt rate was prescribed over an even greater area and mean undercut size was larger. In fact, $Summer_1$ has the lowest mass losses of all the non-control summer simulations, suggesting that mean undercut size is not the most important driver of calving in Elmer/Ice. These results therefore suggest complex frontal morphology may be more important for the promotion of calving events. A two-dimensional modelling study by Ma and Bassis (2019) came to a similar conclusion; both the magnitude and spatial distribution of submarine melt rates were found to be of great importance in determining overall frontal ablation rates.

This links to the profiles of frontal morphology in Figure 8, where the profile from $Summer_3$ shows more complexity than the undercuts from other simulations, having two distinct undercut sections. This is a similar geometry to the observational profiles presented by Holmes and others (2023), but modelled undercut sizes appear to be overestimated, perhaps as a consequence of too high melt rates prescribed in the model. However, this comparison is made on the basis of limited observational data, and further mapping of glacier termini may yield more nuanced insights into the size distribution of undercuts at Kronebreen and elsewhere. Despite this, the general geometrical correspondence between the modelled undercuts from $Summer_3$ and the observational profiles presented by Holmes and others (2023) combined with the fact that $Summer_3$ exhibited higher mass losses than the simple parameterisation in $Summer_1$ shows that including both vertical and horizontal differentiation in submarine melt rates is important for understanding controls on calving and frontal ablation. Comparisons between melt rates in the $Summer_4$ simulation, where a gradual undercut was prescribed, and the $Summer_{1,\,2\text{ and }3}$ simulations suggest that the angularity of the undercut may play a role in determining the level of calving. As such, further investigation of undercut geometries using more nuanced scenarios is necessary to fully tease apart from the relationship between undercut geometry and calving at Kronebreen.

In terms of summertime margin change, the simulations showed more retreat than has been observed, with retreat rates of up to 9 m d^{-1} in the central parts of the glacier. In contrast, observational data from summer 2016 shows peak retreat rates of ~4 m d^{-1} (Holmes and others, 2019). This suggests that the model configuration simulates too much retreat, which is likely related to the very high modelled calving losses. When combined with the fact that the mean modelled undercuts were too large (at least at non-plume locations), it can be seen that there is overestimation of summer frontal ablation in the model set-up.

Despite discrepancies between the model results and observations, the data presented here provides evidence for a strong sensitivity of modelled calving to both the magnitude of and spatial variation in prescribed submarine melt rates.

Links between frontal ablation and glacier dynamics

Research focusing on glaciers with floating ice tongues has demonstrated the potential for velocity increases after large calving events (e.g. Hill and others, 2018), but less work has been conducted on grounded glaciers.

The elevated velocities in the $Summer_{1,\,2,\,3\text{ and }4}$ compared to $Summer_{control}$ highlight the importance of melt and calving for glacier dynamics. These elevated velocities, which correspond well to observations of Kronebreen's summer flow speed during the summers of both 2013 and 2016 (Luckman and others, 2015; Holmes and others, 2019), can be attributed to high levels of frontal ablation rather than summer basal friction or SMB. This is because the $Summer_{control}$ simulation also used the inverted summer basal friction values and the summer SMB values but exhibited much lower frontal velocities. Consequently, the results suggest that the modelled frontal velocities at Kronebreen are primarily impacted by variations in frontal ablation or the choice of a particular sliding law rather than by seasonal variations in basal friction. This suggests that the use of well constrained submarine melt scenarios or a coupled glacier-ocean model is vital for producing accurate simulations of Kronebreen's behaviour.

When considering maximum frontal velocities, the data in Figure 6 show a correlation between modelled calving events and the step increases in maximum modelled velocity. This provides clear evidence for calving events leading to a glacier dynamic response (acceleration). However, the fact that this pattern is not seen in the mean frontal velocities indicates that the velocity increases are likely localised to the area where calving occurred. In addition, some simulations show small decreases in maximum velocity, which is likely due to the fastest flowing areas of the calving front being lost in a calving event.

The impact of sea-ice back pressure on Kronebreen's behaviour

The impact of sea-ice back pressure at Kronebreen was investigated through the suite of winter simulations, where little evidence was found for a strong impact of sea ice on Kronebreen's behaviour. The margin change and velocities of all the winter simulations were similar (Figs 4, 5), as was both the overall mass loss and contribution of calving and submarine melt to mass loss (Fig. 7). However, the $Winter_{control}$ simulation did have overall higher mass losses than all the other winter simulations, which could be an indication that sea-ice back pressure is having a small impact on Kronebreen. Despite this, with recent studies showing the maximum sea-ice thickness in Kongsfjorden has only been ~0.2 m since 2006 it seems unlikely that the inclusion of sea-ice back pressure at Kronebreen is significant for model behaviour (Pavlova and others, 2019). This is in contrast to studies in localities such as Greenland, where the absence or presence of ice melange has been found to be important for frontal ablation and overall dynamics of marine-terminating glaciers (Todd and others, 2018; Barnett and others, 2022).

Observations of winter margin change from 2016 to 2017 indicate small advances of up to 3 m d^{-1} are possible, but retreat remains common during the period December to February (Holmes and others, 2019). In the model, which simulates the period December to February, both retreat and advance were seen across different sections of the margin. As such, the model did not show as much retreat as the observations, suggesting that the level of frontal ablation would need to be increased if aiming at replicating glacier behaviour during this time period as exactly as possible.

https://doi.org/10.1017/jog.2023.94 Published online by Cambridge University Press

The impact of sliding law on model behaviour

The impact of sliding law on model behaviour can be assessed by comparing the Weertman summer simulations with the Coulomb summer simulations. Here, the overall retreat rates were similar between all the simulations, with the key exception that both velocities and retreat were much higher in $\text{Summer}_{\text{CoulombControl}}$ than in $\text{Summer}_{\text{control}}$. This suggests that the Coulomb sliding law leads to higher velocities, calving, and retreat than the Weertman sliding law in this model set-up – in the absence of submarine melt. As a result, it can be seen that the choice of sliding law exerts a significant influence on model behaviour, but that this influence is not so easily be seen when submarine melt is included in the set-up.

As such, submarine melt appears to be a key determinant of model behaviour, with the sliding law exerting a significant, but secondary, control on modelled velocities and calving.

Model limitations

The model used here simulates only viscous material behaviour, but calving is known to be related to visco-elastic deformation (Reeh and others, 2003) as well as damage mechanics (Krug and others, 2015) and has been previously investigated using both continuum and particle models (e.g. Benn and others, 2017; Vallot and others, 2018). However, the use of a viscous model allowed for several months of simulation time and thus for the development of Kronebreen during both the summer and winter seasons to be investigated.

The set-up also does not include any plume modelling, but rather parameterises the submarine melt rates based on observational data relating to water temperatures and frontal morphology, as well as previously published estimates of frontal ablation at Kronebreen. This was useful in allowing for the sensitivity of the model to different levels of parameterisation complexity to be examined, but the inclusion of a specific plume model linked to subglacial discharge (e.g. as described by Cook and others, 2020) or with an entire fjord component (e.g. De Andrés and others, 2018; Gladstone and others, 2021) would be a useful next step and ensure a high accuracy in modelled frontal geometry – something that the results presented here suggest the model is sensitive to. In addition, most of the parameterisations used here likely lead to a more angular modelled undercut than would likely be found in reality – something which impacts the stress regime and, subsequently, modelled calving. These unphysically high stresses may be partly responsible for the dominance of calving as the primary mass loss process in the summer simulations and, while likely lead to an overestimation of calving, are useful in indicating the sensitivity of modelled calving to undercut development and geometry. The additional inclusion of a simulation with a more gradual undercut helps to elucidate the impact of the melt scenarios used, and the evaluation of simple melt parameterisations such as those employed here is useful in informing how melt can be included in longer-term models where computational costs need to be kept to a minimum.

Only one basal inversion was performed for each season, with a reasonable correspondence found between the modelled velocities and previously published observations of frontal velocity at Kronebreen. Previous research has demonstrated that sliding laws based on inversions and Weertman sliding can be problematic at Kronebreen due to high spatio-temporal variability in basal friction (Vallot and others, 2017). However, although these issues preclude the use of a temporally or spatially fixed basal friction field, specific inversions done for each season in each given year were found to show a generally good fit (Vallot and others, 2017). Thus, we here use inverted friction fields for each 3 month simulation based upon velocities from the same time period, in order to reduce any errors associated with the high variability in basal friction at Kronebreen. In addition, we also run summer simulations with an effective pressure-based Coulomb sliding law, allowing for evaluation of the sensitivity of the model results to the choice of sliding law. It should also be noted that, while a Coulomb sliding law negates some of the issues associated with the Weertman sliding law, it can also be problematic due to issues in constraining values of basal water pressures (Vallot and others, 2017).

Due to the limitations listed above, these simulations should be viewed as indicative results which provide information on how sensitive the calving model in Elmer/Ice is to different submarine melt and sea-ice back pressure scenarios. The results can help provide insight into the influence that different submarine melt parameterisations can have on modelled calving activity and dynamics and provide a motivation for further research (both modelling and observational), but do not attempt to provide a realistic analogue of conditions during 2016–17.

Conclusions

The differences between the summer and winter simulations show clear seasonal variations in velocities and frontal ablation rates. Through comparison with the control simulations, it appears clear that submarine melt is a key driver of seasonal variation in model behaviour and that elevated levels of submarine melt can have a significant impact on modelled calving activity and glacier dynamics. This can take the form of consistently high summer velocities across the entire frontal area, or can be related to localised short-term accelerations following individual calving events.

The choice of submarine melt parameterisation is important, with the inclusion of vertical and horizontal differentiation leading to higher calving losses even in the context of lower mean submarine melt rates. This highlights the need for well constrained submarine melt rates at different depths, either from targeted field sampling or the use of high-resolution fjord or ocean models. The choice of sliding law is also important, with significant variations in dynamics and calving losses being seen in control simulations with different sliding laws prescribed. As such, longer-term prognostic simulations need to account for both spatio-temporal variations in submarine melt and sliding law related uncertainties in order to be able to accurately model retreat rates and variations in glacier dynamics.

Supplementary material. The supplementary material for this article can be found at https://doi.org/10.1017/jog.2023.94

Acknowledgements. The study was funded by the Swedish Research Council FORMAS under grant 2017-00665 awarded to N.K. The simulations were enabled by resources provided via the Bolin Centre for Climate Research, through the Swedish National Infrastructure for Computing (SNIC) at the National Supercomputer Centre (NSC) partially funded by the Swedish Research Council through grant agreement No. 2018-05973. The authors are grateful to Brice Noël for the daily SMB data used in the model set-up. The code for the Elmer/Ice model is available at github.com/ElmerCSC/elmerfem and the SMB data are available online at https://doi.pangaea.de/10.1594/PANGAEA.920984.

References

An L and 5 others (2021) Ocean melting of the Zachariae Isstrøm and Nioghalvfjerdsfjorden glaciers, northeast Greenland. *Proceedings of the National Academy of Sciences of the United States of America* **118**(2), e2015483118. doi:10.1073/pnas.201548311

Barnett J, Holmes FA and Kirchner N (2022) Modelled dynamic retreat of Kangerlussuaq Glacier, East Greenland, strongly influenced by the

consecutive absence of an ice mélange in Kangerlussuaq fjord. *Journal of Glaciology* **69**, 1–12. doi:10.1017/JOG.2022.70

Bartholomaus TC, Larsen CF and O'Neel S (2013) Does calving matter? Evidence for significant submarine melt. *Earth and Planetary Science Letters* **380**, 21–30. doi:10.1016/j.epsl.2013.08.014

Barton BI and 5 others (2018) Observed Atlantification of the Barents Sea causes the Polar Front to limit the expansion of winter sea ice. *Journal of Physical Oceanography* **48**, 18–0003. doi:10.1175/JPO-D-18-0003.1

Benn DI, Cowton T, Todd J and Luckman A (2017) Glacier calving in Greenland. *Current Climate Change Reports* **3**, 282–290. doi:10.1007/s40641-017-0070-1

Benn DI, Warren CR and Mottram RH (2007) Calving processes and the dynamics of calving glaciers. *Earth-Science Reviews* **82**(3–4), 143–179. doi:10.1016/J.EARSCIREV.2007.02.002

Błaszczyk M, Jania J and Res JH (2009) Tidewater glaciers of Svalbard: recent changes and estimates of calving fluxes. *Polish Polar Research* **30**(2), 85–142.

Carr J and 9 others (2015) Basal topographic controls on rapid retreat of Humboldt Glacier, northern Greenland. *Journal of Glaciology* **61**(225), 137–150. doi:10.3189/2015JoG14J128

Christoffersen P and 7 others (2011) Warming of waters in an East Greenland fjord prior to glacier retreat: mechanisms and connection to large-scale atmospheric conditions. *The Cryosphere* **5**(3), 701–714. doi:10.5194/tc-5-701-2011

Clason CC, Applegate PJ and Holmlund P (2014) Modelling Late Weichselian evolution of the Eurasian ice sheets forced by surface meltwater-enhanced basal sliding. *Journal of Glaciology* **60**(219), 29–40. doi:10.3189/2014JOG13J037

Cook SJ, Christoffersen P, Todd J, Slater D and Chauché N (2020) Coupled modelling of subglacial hydrology and calving-front melting at Store Glacier, West Greenland. *The Cryosphere* **14**(3), 905–924. doi:10.5194/TC-14-905-2020

Cottier F and 5 others (2005) Water mass modification in an Arctic fjord through cross-shelf exchange: the seasonal hydrography of Kongsfjorden, Svalbard. *Journal of Geophysical Research* **110**, C12005. doi:10.1029/2004JC002757

De Andrés E and 5 others (2018) A two-dimensional glacier-fjord coupled model applied to estimate submarine melt rates and front position changes of Hansbreen, Svalbard. *Journal of Glaciology* **68**, 745–758. doi:10.1017/jog.2018.61

Deschamps-Berger C and 5 others (2019) Closing the mass budget of a tidewater glacier: the example of Kronebreen, Svalbard. *Journal of Glaciology* **65**(249), 136–148. doi:10.1017/JOG.2018.98

Gagliardini O and 14 others (2013) Capabilities and performance of Elmer/Ice, a new-generation ice sheet model. *Geoscientific Model Development* **6**(4), 1299–1318. doi:10.5194/GMD-6-1299-2013

Geyman EC, J J van Pelt W, Maloof AC, Aas HF and Kohler J (2022) Historical glacier change on Svalbard predicts doubling of mass loss by 2100. *Nature* **601**(7893), 374–379. doi:10.1038/s41586-021-04314-4

Gladstone R and 12 others (2021) The framework for ice sheet-ocean coupling (FISOC) V1.1. *Geoscientific Model Development* **14**(2), 889–905. doi:10.5194/GMD-14-889-2021

Hill EA, Hilmar Gudmundsson G, Rachel Carr J and Stokes CR (2018) Velocity response of Petermann Glacier, northwest Greenland, to past and future calving events. *The Cryosphere* **12**(12), 3907–3921. doi:10.5194/tc-12-3907-2018

Holmes FA, van Dongen E, Noormets R, Pe¸tlicki M and Kirchner N (2023) Modelled 3D calving at Kronebreen, Svalbard, driven by tidal fluctuations and frontal melt. *The Cryosphere* **17**, 1853–1872. doi:10.5194/tc-17-1853-2023

Holmes FA, Kirchner N, Kuttenkeuler J, Krützfeldt J and Noormets R (2019) Relating ocean temperatures to frontal ablation rates at Svalbard tidewater glaciers: insights from glacier proximal datasets. *Scientific Reports* **9**(1), 9442. doi:10.1038/s41598-019-45077-3

How P and 8 others (2019) Calving controlled by melt-under-cutting: detailed calving styles revealed through time-lapse observations. *Annals of Glaciology*, 20–31. doi:10.1017/aog.2018.28

Jakobsson M and 30 others (2020) Ryder Glacier in northwest Greenland is shielded from warm Atlantic water by a bathymetric sill. *Communications Earth & Environment* **1**(1), 1–10. doi:10.1038/s43247-020-00043-0

Joughin I, Smith BE and Schoof CG (2019) Regularized coulomb friction laws for ice sheet sliding: application to Pine Island Glacier, Antarctica. *Geophysical Research Letters* **46**(9), 4764–4771. doi:10.1029/2019GL082526

Köhler A and 5 others (2019) Contribution of calving to frontal ablation quantified from seismic and hydroacoustic observations calibrated with lidar measurements. *The Cryosphere* **13**(11), 3117–3137. doi:10.5194/tc-13-3117-2019

Krug J, Durand G, Gagliardini O and Weiss J (2015) Modelling the impact of submarine frontal melting and ice mélange on glacier dynamics. *The Cryosphere* **9**(3), 989–1003. doi:10.5194/TC-9-989-2015

Lemos A and 5 others (2018) Ice velocity of Jakobshavn Isbrae, Petermann Glacier, Nioghalvfjerdsfjorden, and Zachariae Isstrøm. *The Cryosphere* **12**, 2087–2097. doi:10.5194/tc-12-2087-2018

Luckman A and 5 others (2015) Calving rates at tidewater glaciers vary strongly with ocean temperature. *Nature Communications* **6**(1), 1–7. doi:10.1038/ncomms9566

Ma Y and Bassis JN (2019) The effect of submarine melting on calving from marine terminating glaciers. *Journal of Geophysical Research: Earth Surface* **124**, 2018JF004820. doi:10.1029/2018JF004820

Moore JC, Grinsted A, Zwinger T and Jevrejeva S (2013) Semiempirical and process-based global sea level projections. *Reviews of Geophysics* **51**(3), 484–522. doi:10.1002/rog.20015

Motyka RJ, Hunter L, Echelmeyer KA and Connor C (2003) Submarine melting at the terminus of a temperate tidewater glacier, LeConte Glacier, Alaska, U.S.A. *Annals of Glaciology* **36**, 57–65. doi:10.3189/172756403781816374

Moyer AN, Nienow PW, Gourmelen N, Sole AJ and Slater DA (2017) Estimating spring terminus submarine melt rates at a Greenlandic tidewater glacier using satellite imagery. *Frontiers in Earth Science* **5**, doi:10.3389/feart.2017.00107

Noël B, van de Berg WJ, Lhermitte S and van den Broeke MR (2019) Rapid ablation zone expansion amplifies north Greenland mass loss. *Science Advances* **5**(9). doi:10.1126/sciadv.aaw0123

Noël BPY and 10 others (2020) Annual surface mass balance (SMB) and components of Svalbard glaciers statistically downscaled to 500 m spatial resolution (1958–2018).

O'Leary M and Christoffersen P (2013) Calving on tidewater glaciers amplified by submarine frontal melting. *The Cryosphere* **7**(1), 119–128. doi:10.5194/tc-7-119-2013

Pavlova O, Gerland S and Hop H (2019) Changes in sea-ice extent and thickness in Kongsfjorden, Svalbard (2003–2016). In Hop H and Wiencke C (eds), *The Ecosystem of Kongsfjorden, Svalbard. Advances in Polar Ecology*, vol 2. Cham: Springer, pp. 105–136. doi:10.1007/978-3-319-46425-1_4

Polyakov IV and 15 others (2017) Greater role for Atlantic inflows on sea-ice loss in the Eurasian Basin of the Arctic Ocean. *Science* **356**(6335), 285–291. doi:10.1126/science.aai8204

Promińska A, Cisek M and Walczowski W (2017) Kongsfjorden and Hornsund hydrography – comparative study based on a multiyear survey in fjords of west Spitsbergen. *Oceanologia* **59**(4), 397–412. doi:10.1016/J.OCEANO.2017.07.003

Reeh N, Christensen EL, Mayer C and Olesen OB (2003) Tidal bending of glaciers: a linear viscoelastic approach. *Annals of Glaciology* **37**, 83–89. doi:10.3189/172756403781815663

Schuler TV and 12 others (2020) Reconciling Svalbard glacier mass balance. *Frontiers in Earth Science* **8**, 156. doi:10.3389/feart.2020.00156

Shepherd A and 80 others (2018) Mass balance of the Antarctic ice sheet from 1992 to 2017. *Nature* **558**(7709), 219–222. doi:10.1038/s41586-018-0179-y

Slater DA and Straneo F (2022) Submarine melting of glaciers in Greenland amplified by atmospheric warming. *Nature Geoscience* **15**(10), 794–799. doi:10.1038/s41561-022-01035-9

Svendsen H and 14 others (2002) The physical environment of Kongsfjorden–Krossfjorden, an Arctic fjord system in Svalbard. *Polar Research* **21**(1), 133–166. doi:10.1111/j.1751-8369.2002.tb00072.x

Todd J and Christoffersen P (2014) Are seasonal calving dynamics forced by buttressing from ice mélange or undercutting by melting? Outcomes from full-Stokes simulations of Store Glacier, West Greenland. *The Cryosphere* **8**(6), 2353–2365. doi:10.5194/tc-8-2353-2014

Todd J and 10 others (2018) A full-Stokes 3-D calving model applied to a large Greenlandic Glacier. *Journal of Geophysical Research: Earth Surface* **123**(3), 410–432. doi:10.1002/2017JF004349

Todd J, Christoffersen P, Zwinger T, Räback P and Benn DI (2019) Sensitivity of a calving glacier to ice–ocean interactions under climate

https://doi.org/10.1017/jog.2023.94 Published online by Cambridge University Press

change: new insights from a 3-D full-Stokes model. *The Cryosphere* **13**(6), 1681–1694. doi:10.5194/TC-13-1681-2019

Vallot D and 9 others (2017) Basal dynamics of Kronebreen, a fast-flowing tidewater glacier in Svalbard: non-local spatio-temporal response to water input. *Journal of Glaciology* **63**(242), 1012–1024. doi:10.1017/jog.2017.69

Vallot D and 9 others (2018) Effects of undercutting and sliding on calving: a global approach applied to Kronebreen, Svalbard. *The Cryosphere* **12**(2), 609–625. doi:10.5194/tc-12-609-2018

Van Pelt WJJ and 5 others (2012) Simulating melt, runoff and refreezing on Nordenskiöldbreen, Svalbard, using a coupled snow and energy balance model. *The Cryosphere* **6**, 641–659. doi:10.5194/tc-6-641-2012

Vihtakari M and 8 others (2018) Black-legged kittiwakes as messengers of Atlantification in the Arctic. *Scientific Reports* **8**(1), 1178. doi:10.1038/s41598-017-19118-8

Weertman J (1974) Stability of the junction of an ice sheet and an ice shelf. *Journal of Glaciology* **13**(67), 3–11. doi:10.3189/S0022143000023327

https://doi.org/10.1017/jog.2023.94 Published online by Cambridge University Press